

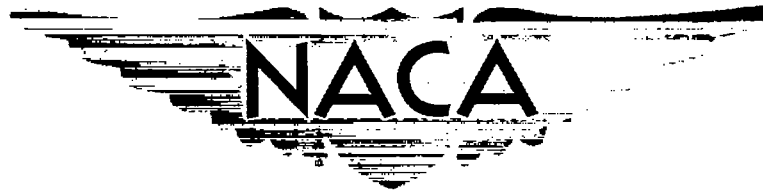
NACA RM A58A08

6525

~~CONFIDENTIAL~~9024
MAR 17 1958

0143478

TECH LIBRARY KAFB, NM



RESEARCH MEMORANDUM

AFOSR

TECHNICAL LIBRARY

AFL 2291

EXPERIMENTAL LIFT-DRAG RATIOS FOR TWO FAMILIES OF WING-BODY COMBINATIONS AT SUPERSONIC SPEEDS

By Leland H. Jorgensen

Ames Aeronautical Laboratory
Moffett Field, Calif.Classification ~~confidential~~ (or changed to UNCLASSIFIED)By authority of NASA "TPA #66" - 1 MAR 1962
(OFFICER AUTHORIZED TO CHANGE)By N. G. G. F. R. E. I.
NAME ANDA/SC
GRADE OF OFFICER MAKING CHANGE)16F1962
DATE

This material contains information affecting the National Defense of the United States within the meaning of the espionage laws, Title 18, U.S.C., Secs. 793 and 794, the transmission or revelation of which in any manner to an unauthorized person is prohibited by law.

NATIONAL ADVISORY COMMITTEE
FOR AERONAUTICS

WASHINGTON

March 10, 1958

~~CONFIDENTIAL~~



0143478

NATIONAL ADVISORY COMMITTEE FOR AERONAUTICS

RESEARCH MEMORANDUMEXPERIMENTAL LIFT-DRAG RATIOS FOR TWO FAMILIES OF WING-
BODY COMBINATIONS AT SUPERSONIC SPEEDS

By Leland H. Jorgensen

SUMMARY

Experimental force and moment characteristics, including lift-drag ratios, have been measured and briefly studied for two families of wing-body combinations. One family consisted of essentially arrow wings with half conical bodies. For these arrow-winged configurations the wing vertex coincided with the body nose, and the wing trailing edge at the root coincided with the body base. The effect of increasing body volume and changing the cross section from circular to elliptical has been studied for free-stream Mach numbers, M_∞ , of 2.94 and 3.88. The Reynolds numbers, based on body length, were 9.1×10^6 and 5.4×10^6 , respectively. The highest maximum lift-drag ratios measured for these configurations were 7.3 at $M_\infty = 2.94$ and 6.8 at $M_\infty = 3.88$.

The other family of wing-body combinations consisted of a fineness-ratio-12 body of revolution alone and with flat-plate triangular wings of aspect ratios ranging from 0.375 to 1.8. The body alone and the triangular-winged configurations were tested at a Mach number of 2.94 and a Reynolds number of 12.0×10^6 , based on body length. The highest maximum lift-drag ratio measured was 7.1, obtained using a wing of aspect ratio 1.414.

INTRODUCTION

At supersonic speeds, as well as at subsonic speeds, the range of an aircraft in relatively steady level flight depends on lift-drag ratio. To obtain high lift-drag ratios, several investigators have studied configurations employing wedges or a half conical body situated beneath a wing of essentially arrow plan form (refs. 1 to 3). Shape variables studied have included wing plan form, wing leading-edge sweep, body profile shape, and body fineness ratio. Most of the models tested have consisted of half circular cones mounted beneath almost flat arrow wings, with the wing and cone vertices coinciding. In the present

investigation, additional tests have been made which show the effect on lift-drag ratio of increasing body volume and changing cross section from circular to elliptical. These tests were made for Mach numbers of 2.94 and 3.88.

In addition to tests of flat-top arrow-winged configurations, tests also have been made of a family of wing-body combinations employing a low-drag body of revolution with flat triangular wings. The effect on lift-drag ratio of increasing wing aspect ratio in successive steps from 0 to 1.8 has been measured for a Mach number of 2.94. The purpose of this report is to present and discuss briefly aerodynamic data, including lift-drag ratios, for both the flat-top arrow-winged configurations and the more conventional triangular-winged configurations.

SYMBOLS

A	aspect ratio of triangular-winged configurations, $\frac{(b-d)^2}{A_w}$
A_p	plan area (including that of body)
A_w	exposed wing area of two panels
b	wing span, body included
C_D	drag coefficient, $\frac{D}{q_\infty A_p}$
C_{D_0}	drag coefficient at zero lift
C_L	lift coefficient, $\frac{L}{q_\infty A_p}$
C_m	pitching-moment coefficient about body base, $\frac{\text{pitching moment}}{q_\infty A_p l}$
D	drag
d	body base diameter
l	body length
l_n	body nose length
L	lift
$\left(\frac{L}{D}\right)_{\max}$	maximum lift-drag ratio

M_∞	free-stream Mach number
q_∞	free-stream dynamic pressure
R	Reynolds number based on body length
r	local body radius
x, y, z	Cartesian coordinates as shown in figure 1
x_p	center of pressure measured from vertex of body nose
α	angle of attack measured with respect to lower surface of wing for models 1, 2, 3, and 4 and with respect to longitudinal axis for other models (see fig. 1)
Λ	sweep angle

The positive directions of the angles and coefficients are shown in figure 1.

APPARATUS AND TESTS

Wind Tunnels

The experimental investigation was conducted in the Ames 1- by 3-foot supersonic wind tunnels no. 1 and no. 2. Tunnel no. 1 is a closed-circuit continuous-operation type and is equipped with a flexible-plate nozzle that provides a variation of Mach number from 1.4 to 4.0. The Reynolds number is changed by varying the total pressure within the approximate limits of 1/5 of an atmosphere to 4 atmospheres. Tunnel no. 2 is a non-return, intermittent-operation type and is also equipped with a flexible-plate nozzle that provides a variation of Mach number from 1.4 to 3.8. Air for this tunnel is obtained from the Ames 12-foot wind tunnel at a pressure of about 5 atmospheres and is expanded through the nozzle to the atmosphere. Changes in Reynolds number are obtained by varying the total pressure.

The water content of the air in both the 1- by 3-foot wind tunnels is maintained at less than 0.0003 pound of water per pound of dry air. Consequently, the effect of humidity on the flow is negligible.

Models

The models tested are shown in figure 2. In figure 2(a), elevation, bottom, and end views of the arrow-winged configurations are shown. For

these models the wings were identical, all wing sections being essentially simple wedges slightly less than 2 percent thick in streamwise planes. The leading edges of the wings were rounded with a radius of 0.003 inch. Differences in the models resulted only from changes in body shape. Model 1, which was geometrically similar to model 5 of reference 3, had a body consisting of half of a fineness-ratio-5 cone (semivertex angle of 5.71°) mounted beneath the wing. Model 2 was identical to model 1 except for the addition of a half cylindrical afterbody which increased the body volume by about 41 percent. Models 3 and 4 had the same longitudinal distribution of cross-sectional area, and hence total volume, as model 2. The body of model 3, which was mounted beneath the wing, was half of a cone-cylinder of elliptic cross section with a major-to-minor axis ratio of 6. For model 4, half of the body volume was placed under the wing in a semicircular cone-cylinder and half above the wing in a semielliptical cone-cylinder.

All of the triangular-winged configurations (fig. 2(b)) had a fineness-ratio-12 body (B_1) consisting of a $3/4$ -power nose (approximate Newtonian minimum-drag shape) of fineness ratio 5 and a cylindrical afterbody of fineness ratio 7. Five triangular wings having aspect ratios from 0.375 to 1.800 were tested with body B_1 . These wings are identified in figure 2(b) by W_1 , W_2 , W_3 , W_4 , and W_5 . The wing sections were flat plates with leading and trailing edges beveled to small radii.

Pertinent geometric properties of all the models tested, such as plan area and body volume, are given in table I. All of the models were constructed of steel and were sting supported from the rear.

Tests

Force tests.- Balance measurements of lift, drag, and pitching moment were obtained in tunnel no. 2 for all the models at a free-stream Mach number of 2.94. For the arrow-winged configurations the Reynolds number, based on body length, was 9.1×10^6 , and for the triangular-winged configurations it was 12.0×10^6 . Data also were obtained in tunnel no. 1 for the arrow-winged configurations at a Mach number of 3.88 and a Reynolds number of 5.4×10^6 . The angle-of-attack range for the arrow-winged configurations was from -6° to 6° and for the triangular-winged configurations from 0° to 16° .

Base pressures from eight orifices spaced around the inside of the base periphery of each model were measured by photographic recording from a multiple-tube manometer board. The repeatability of the force and base pressure measurements was checked by making reruns for several configurations.

Sublimation tests.- The sublimation technique (ref. 4) was used for determining boundary-layer transition. The models, which were initially painted black, were sprayed with a saturated solution of tetrachlorobenzene in benzene. This solution dries on contact with the model surface and presents a white appearance. The wind tunnel is operated and, as the process of sublimation takes place with the model in the tunnel, evidence of boundary-layer transition appears on the model. (Other solutions, such as acenaphthene and azobenzene dissolved in petroleum ether, can be used for slower rates of sublimation.) Turbulent boundary layers, associated with regions of high surface shear, show up as dark areas; whereas regions of laminar flow and separation remain white. Sublimation tests were made in both wind tunnels.

REDUCTION AND ACCURACY OF DATA

All of the force and moment data have been reduced to coefficient form and are referred to the coordinate system shown in figure 1. The base drag was computed using the average base pressure and was subtracted from the total axial-force balance measurement, so that the data presented (except where noted in fig. 7) are for forces ahead of the body base.

The accuracy of the final data is affected by uncertainties in the measurement of the forces and moments, and in the determination of the stream static and dynamic pressures used in reducing the forces and moments to coefficient form. These individual uncertainties led to estimated uncertainties which are listed in the following table:

C_L	± 0.002
C_D	± 0.0002
C_m	± 0.002
L/D	± 2
x_p/l	± 0.02

The values of angle of attack are estimated to be accurate to within $\pm 0.1^\circ$. The variation of the free-stream Mach number in the region of the test models was less than ± 0.02 at both Mach numbers 2.94 and 3.88.

RESULTS AND DISCUSSION

Arrow-Winged Configurations

The aerodynamic characteristics of the arrow-winged configurations are presented in figure 3 for $M_\infty = 2.94$ and $R = 9.1 \times 10^6$ and in figure 4 for $M_\infty = 3.88$ and $R = 5.4 \times 10^6$. The lift, drag, and pitching-moment coefficients for models 1, 2, 3, and 4 are all based on the plan area of

model 1. Differences in forces and moments for the models resulted from differences in the bodies, the wings of these models being identical. Model 2 was the same as model 1 except for the addition of a half cylindrical afterbody which increased the body volume about 41 percent. Models 3 and 4 had the same volume as model 2. The body of model 3, however, was a half cone-cylinder of elliptic cross section. The body of model 4 consisted of a half cone-cylinder of elliptic cross section above the wing and a half cone-cylinder of circular cross section below the wing. The volume above the wing was equal to that below. Models 3 and 4 were constructed with elliptic cross sections as a result of the findings of reference 5. In reference 5 it is shown that, for triangular wings of low aspect ratio mounted on cones, higher lift-drag ratios are obtained with an elliptic cross section with major axis in line with the wings than with a circular cross section. However, the cones studied were of lower fineness ratio than those of this investigation, and hence the lift-drag ratios were all somewhat lower.

As shown in figures 3 and 4, there are no large effects on the lift-drag polars and lift-drag ratios resulting from the changes in body shape for the arrow-winged models. The addition of 41-percent body volume to model 1 resulted in little or no loss in L/D . (Compare results for models 1 and 2 in figs. 3(c) and 4(c).) The highest L/D at $M_{\infty} = 2.94$ was 7.3, obtained with model 4. The highest L/D at $M_{\infty} = 3.88$ was 6.8, obtained with model 3. For all models the lift-drag ratios were higher in the positive angle-of-attack range than in the negative. Thus, the advantage in L/D of flat-top over flat-bottom configurations, attested to in references 1 to 3, is clearly demonstrated. In all tests the boundary-layer flow over the models was essentially turbulent, the length of laminar run being about the same as for the triangular-winged models to be discussed.

Triangular-Winged Configurations

The aerodynamic characteristics of the family of triangular-winged configurations (consisting of a low-drag body with flat triangular wings) are presented in figure 5 for $M_{\infty} = 2.94$ and $R = 12.0 \times 10^6$. The reader is reminded that the lift, drag, and pitching-moment coefficients for each configuration are based on total plan area, including the body. The results should be assessed on the basis of almost a completely turbulent boundary-layer flow over the surface of the models. From sublimation tests it was found that the flow was laminar only over the forward half of the body nose. Photographs of several models taken following the sublimation tests are shown in figure 6.

In figure 5(a) it is clearly evident that the lift effectiveness of a body alone can be appreciably increased with the addition of even wings of very low aspect ratio. For these configurations the lift effectiveness increased with each successive increase in aspect ratio

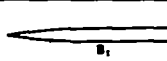

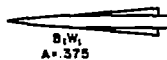


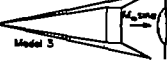




from 0 to 1.8. It is interesting to note that the model with a supersonic leading-edge wing (B_1W_5 , $A = 1.8$) has a slightly higher lift coefficient than the model with essentially a sonic leading-edge wing (B_1W_4 , $A = 1.414$).

The effect of change in aspect ratio on the lift-drag polars and lift-drag ratios is shown in figures 5(b) and 5(c). The zero-lift-drag coefficients were all about the same ($C_{D_0} \approx 0.0060$) for the models with wings of aspect ratios 0.667, 1, and 1.414. For these models, drag due to lift decreased with increase in aspect ratio, and hence lift-drag ratio increased. The model with the wing of aspect ratio 1.414 (B_1W_4) developed the highest maximum lift-drag ratio (about 7.1). Decrease in maximum lift-drag ratio as the wing changes from $A = 1.414$ to $A = 1.8$ can be attributed mainly to an increase in C_{D_0} .

The effect of change in aspect ratio on the pitching moments and centers of pressure is shown in figures 5(d) and 5(e). The center of pressure for the body (B_1) starts on the nose section at zero angle of attack and then moves rearward toward the centroid of the body as the angle of attack is increased. Adding even the smallest wing results in a rearward shift of the center of pressure at all angles of attack. It is also apparent that the addition of wings of even low aspect ratio results in small center-of-pressure travel with angle of attack.

Comparisons of Maximum Lift-Drag Ratios

Maximum lift-drag ratios for all the models tested are summarized in the following table:

	$M_\infty = 2.94$		$M_\infty = 2.94$	$M_\infty = 3.88$
 B_1	3.8	 Model 1	6.9	6.7
 B_1W_1 $A = .375$	5.2	 Model 2	6.9	6.5
 B_1W_2 $A = .667$	5.9	 Model 3	6.9	6.8
 B_1W_3 $A = 1$	6.6	 Model 4	7.3	6.7
 B_1W_4 $A = 1.414$	7.1			
 B_1W_5 $A = 1.800$	6.5			

Maximum lift-drag ratios for the models tested at $M_\infty = 2.94$ are plotted in figure 7. On the left side of the figure is shown the effect of aspect ratio on maximum lift-drag ratio for the triangular-winged configurations. It is seen that $(L/D)_{\max}$ increases with increase in aspect ratio from 0 to 1.414 but decreases with increase in aspect ratio from 1.414 to 1.8.

On the right side of figure 7, maximum lift-drag ratios are plotted as a function of $\frac{(\text{body volume})^{2/3}}{\text{plan area}}$. With this plot the effect of volume carrying capacity on $(L/D)_{\max}$ is demonstrated. As shown for the triangular-winged configuration, $(L/D)_{\max}$ generally increases as $\frac{(\text{body volume})^{2/3}}{\text{plan area}}$ decreases. The theoretical wing alone value of $(L/D)_{\max} = 7.76$ represents the maximum lift-drag ratio which could be expected for a triangular-winged configuration with vanishing body. The wing alone value was computed using linearized (flat plate) wing theory with $C_{D_0} = 0.0060$. This value of C_{D_0} was close to the experimental values for models B_1W_2 , B_1W_3 , and B_1W_4 .

Also demonstrated on the right side of figure 7 is the effect on $(L/D)_{\max}$ of including base drag. Base drags for model 1 and the triangular-winged models were computed using reference 6. The effect of base drag lowers $(L/D)_{\max}$ for model 1 from 6.9 to about 4.9. Although it is more difficult to compute the base drags for models 2, 3, and 4, it was estimated that the maximum lift-drag ratios would be of the order of 5. The inclusion of base drag lowers the magnitude of $(L/D)_{\max}$ by at least 1 for all the configurations studied. However, with proper boattailing of the cylindrical afterbody of the triangular-winged configurations, some loss in $(L/D)_{\max}$ attributed to base drag can be recovered. (Compare curves on the right side of fig. 7.)

CONCLUSIONS

Experimental force and moment characteristics, including lift-drag ratios, have been studied for two families of wing-body combinations. One family consisted of identical arrow wings with half bodies of both circular and elliptic cross section. Tests were made at a Mach number of 2.94 (Reynolds number of 9.1×10^6) and a Mach number of 3.88 (Reynolds number of 5.4×10^6). The other family studied consisted of a low-drag body of revolution with triangular wings of aspect ratios ranging from 0 to 1.8. These configurations were tested at a Mach number of 2.94 (Reynolds number of 12.0×10^6). A brief analysis of the results has led to the following conclusions:

1. For the arrow-winged configurations, the effect on lift-drag ratio resulting from change in body cross-sectional shape is not large.
2. Increasing body volume of an arrow-winged configuration by as much as about 40 percent by addition of a half cylindrical afterbody results in little loss in lift-drag ratio.
3. For the arrow-winged configurations, higher lift-drag ratios were obtained with the flat-top arrangements than with the flat bottom.
4. For the triangular-winged configurations, maximum lift-drag ratio increases with increase in aspect ratio for wings having subsonic leading edges. Maximum lift-drag ratio decreases with increase in aspect ratio as the wing changes from one with essentially a sonic leading edge to one with a supersonic leading edge, the root chord remaining constant.
5. In general, maximum lift-drag ratio increases with decrease in the parameter $\frac{(\text{body volume})^{2/3}}{\text{plan area}}$.

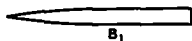
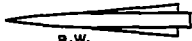


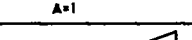

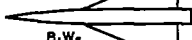
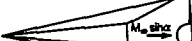

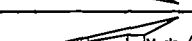
Ames Aeronautical Laboratory
National Advisory Committee for Aeronautics
Moffett Field, Calif., Jan. 8, 1958

REFERENCES

1. Ferri, Antonio, Clarke, Joseph H., and Casaccio, Anthony: Drag Reduction in Lifting Systems by Advantageous Use of Interference. PIBAL Rep. 272, Polytechnic Institute of Brooklyn, Dept. Aero. Engr. and Appl. Mech., May 1955.
2. Eggers, A. J., Jr., and Syvertson, Clarence A.: Aircraft Configurations Developing High Lift-Drag Ratios at High Supersonic Speeds. NACA RM A55L05, 1956.
3. Syvertson, Clarence A., Wong, Thomas J., and Gloria, Hermilo R.: Additional Experiments With Flat-Top Wing-Body Combinations at High Supersonic Speeds. NACA RM A56I11, 1957.
4. Main-Smith, J. D.: Chemical Solids as Diffusible Coating Films for Visual Indications of Boundary-Layer Transition in Air and Water. R. & M. No. 2755, British A.R.C., 1954. (Also A.R.C. Rep. 13,115 and R.A.E. Chem. 466, Feb. 1950)

5. Jorgensen, Leland H.: Elliptic Cones Alone and With Wings at Supersonic Speeds. NACA TN 4045, 1957.
6. Seiff, Alvin, Sandahl, Carl A., Chapman, Dean R., Perkins E. W., and Gowen, Forrest E.: Aerodynamic Characteristics of Bodies at Supersonic Speeds. - A collection of three papers. Pt. 2. NACA RM A51J25, 1951.

TABLE I.- GEOMETRIC PROPERTIES OF TEST MODELS

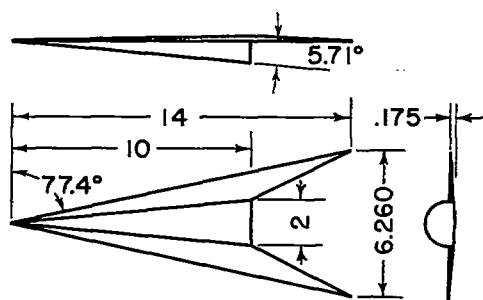
Model	Body length, in.	Plan area, in. ²	Body vol, in. ³	$\frac{(\text{Body vol})^{2/3}}{\text{Plan area}}$	$\frac{\text{Plan area}}{(\text{Body length})^2}$	$\frac{\text{Body vol}}{(\text{Body length})^3}$
 B ₁	15.000	15.40	13.81	0.374	0.068	0.00409
 B ₁ W ₁ A=.375	15.000	21.03	13.81	.274	.094	.00409
 B ₁ W ₂ A=.667	15.000	25.40	13.81	.227	.113	.00409
 B ₁ W ₃ A=1	15.000	30.40	13.81	.189	.135	.00409
 B ₁ W ₄ A=1.414	15.000	36.60	13.81	.157	.163	.00409
 B ₁ W ₅ A=1.800	15.000	42.42	13.81	.136	.188	.00409
 Model 1	10.000	27.30	^a 5.24	.111	.273	.00524
 Model 2	11.373	30.05	^a 7.40	.126	.232	.00503
 Model 3	11.373	30.55	^a 7.40	.124	.236	.00503
 Model 4	11.373	30.55	^a 7.40	.124	.236	.00503

^aThis body volume excludes the volume of the wing extended through the body.

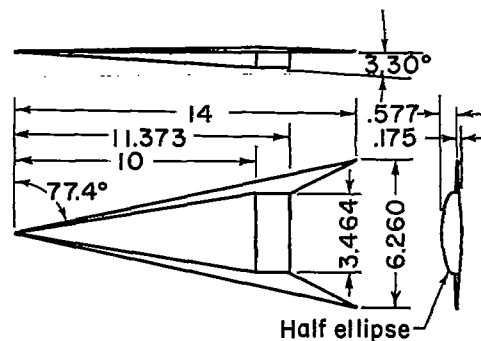




3

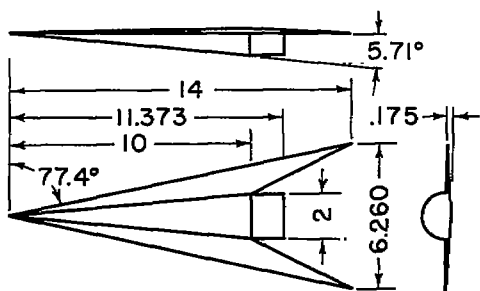


Model 1

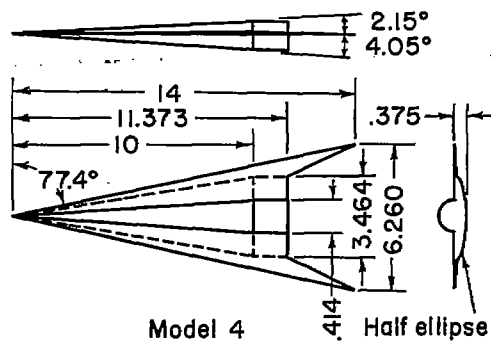


Model 3

Note: All dimensions in inches.
(except as noted)

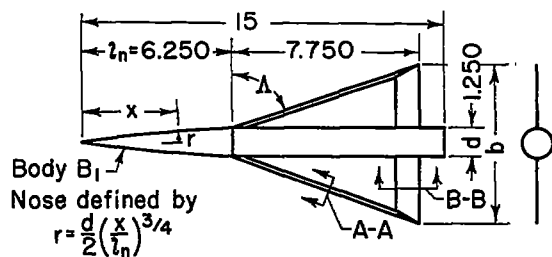


Model 2



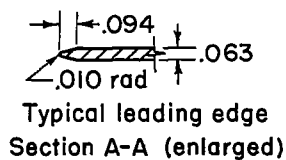
Model 4

(a) Arrow-winged configurations.

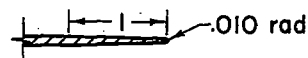


Body B₁
Nose defined by
 $r = \frac{d}{(x/l_n)^{3/4}}$

Wing	b	Δ , deg	A
W ₁	2.702	84.7	0.375
W ₂	3.833	80.5	0.667
W ₃	5.125	76.0	1.000
W ₄	6.725	70.5	1.414
W ₅	8.225	65.8	1.800



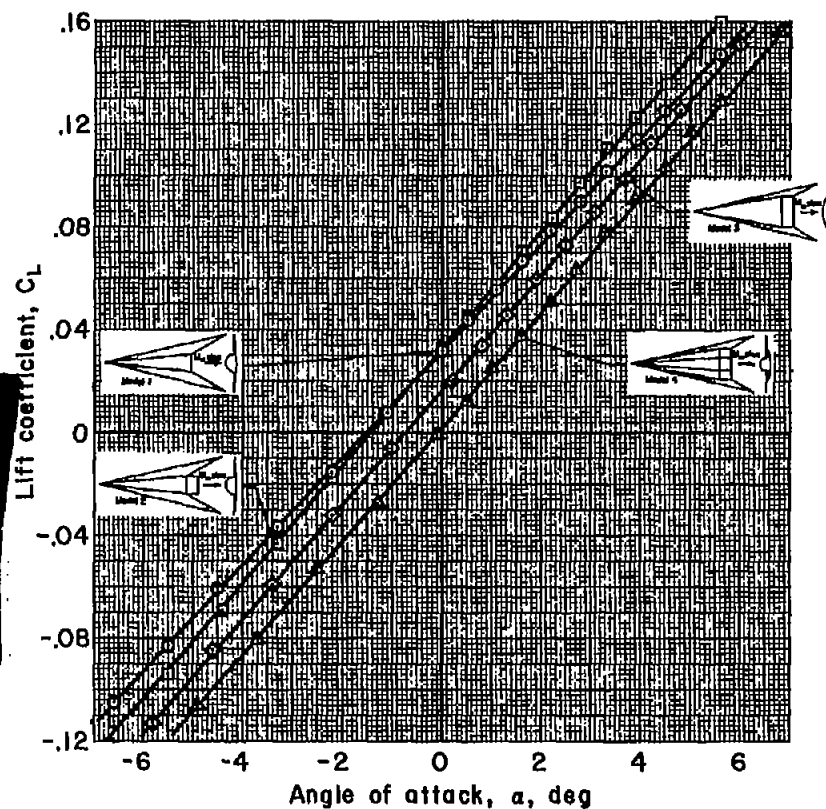
Typical leading edge
Section A-A (enlarged)



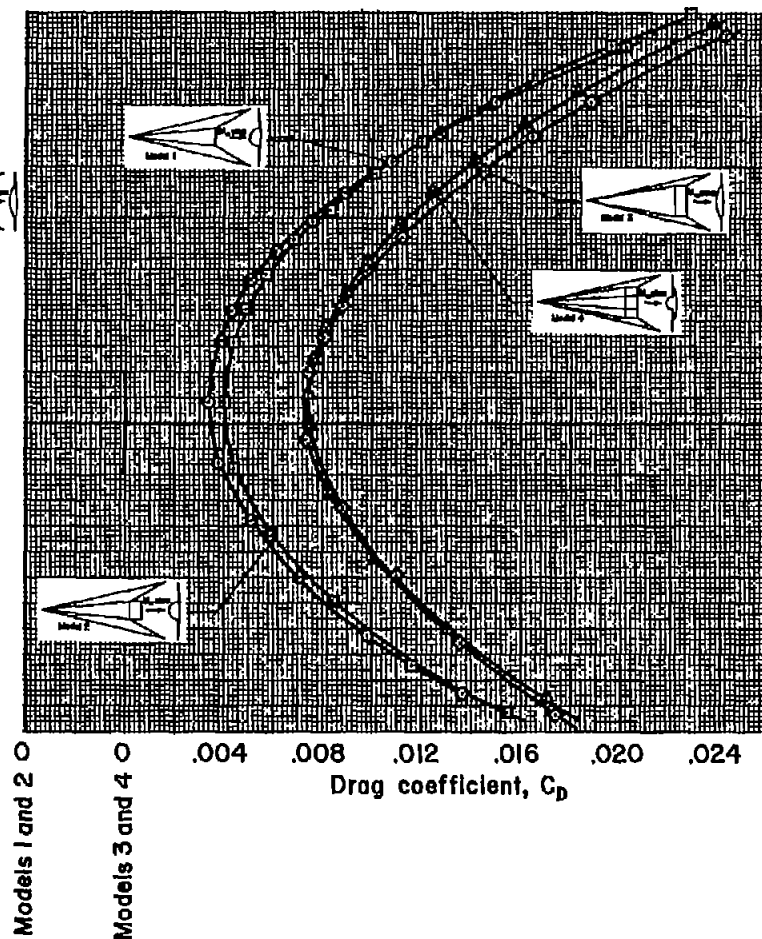
Typical trailing edge
Section B-B (enlarged)

(b) Triangular-winged configurations.

Figure 2.4 Models tested.

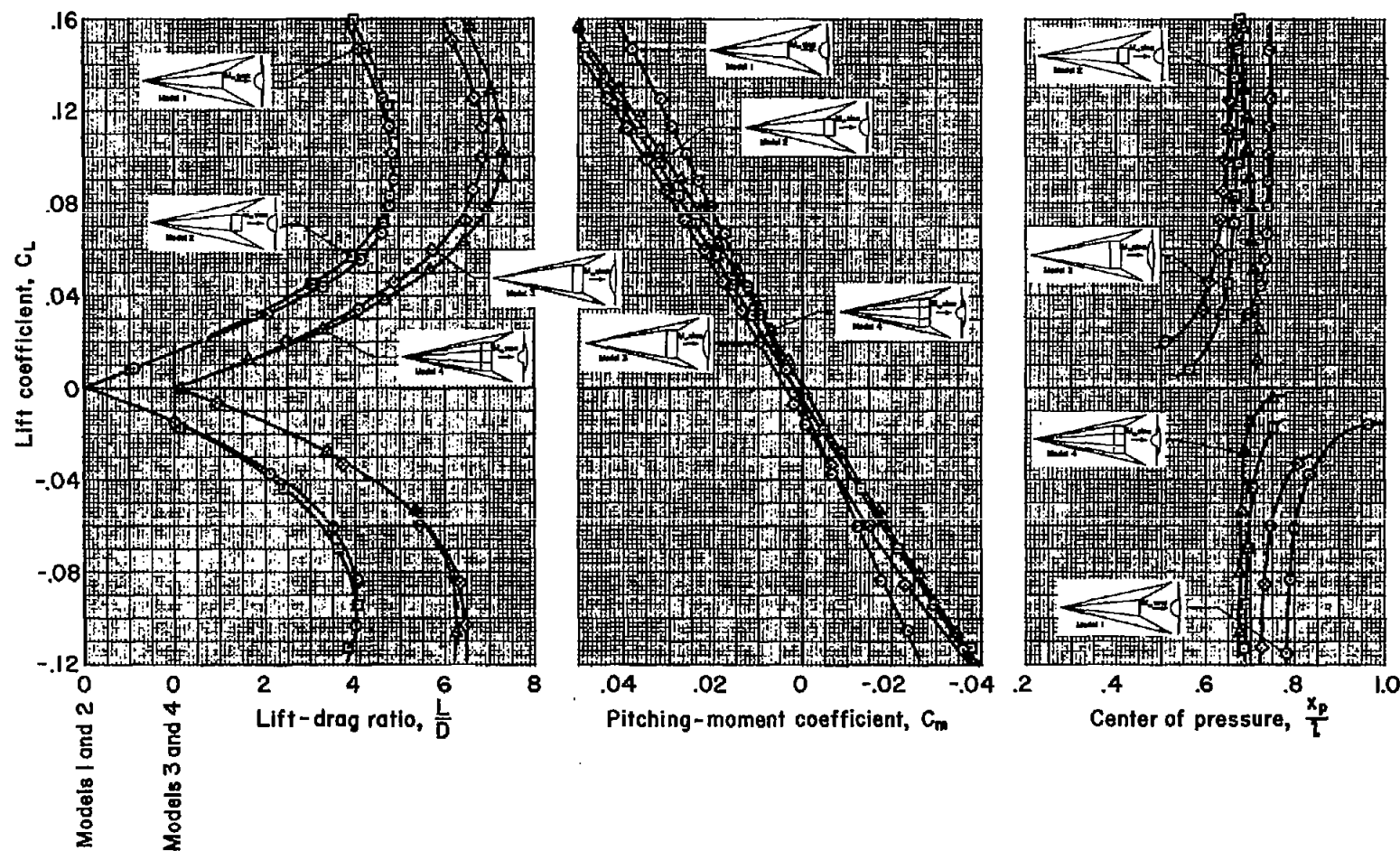


(a) Lift.



(b) Lift-drag polar.

Figure 3.- Aerodynamic characteristics of arrow-winged configurations; $M_\infty = 2.94$, $R = 9.1 \times 10^6$.



(c) Lift-drag ratio.

(d) Pitching moment.

(e) Center of pressure.

Figure 3.- Concluded.

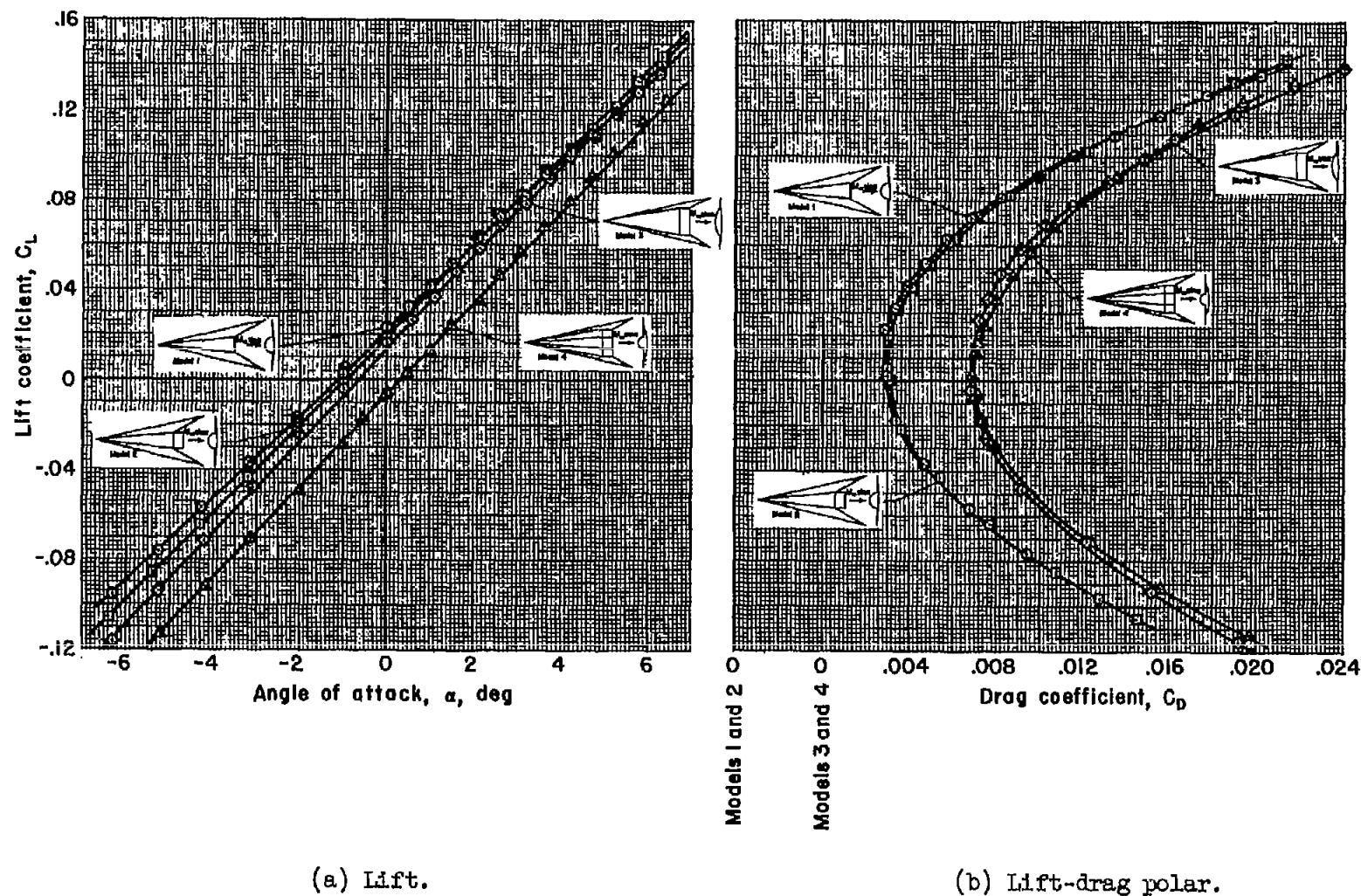
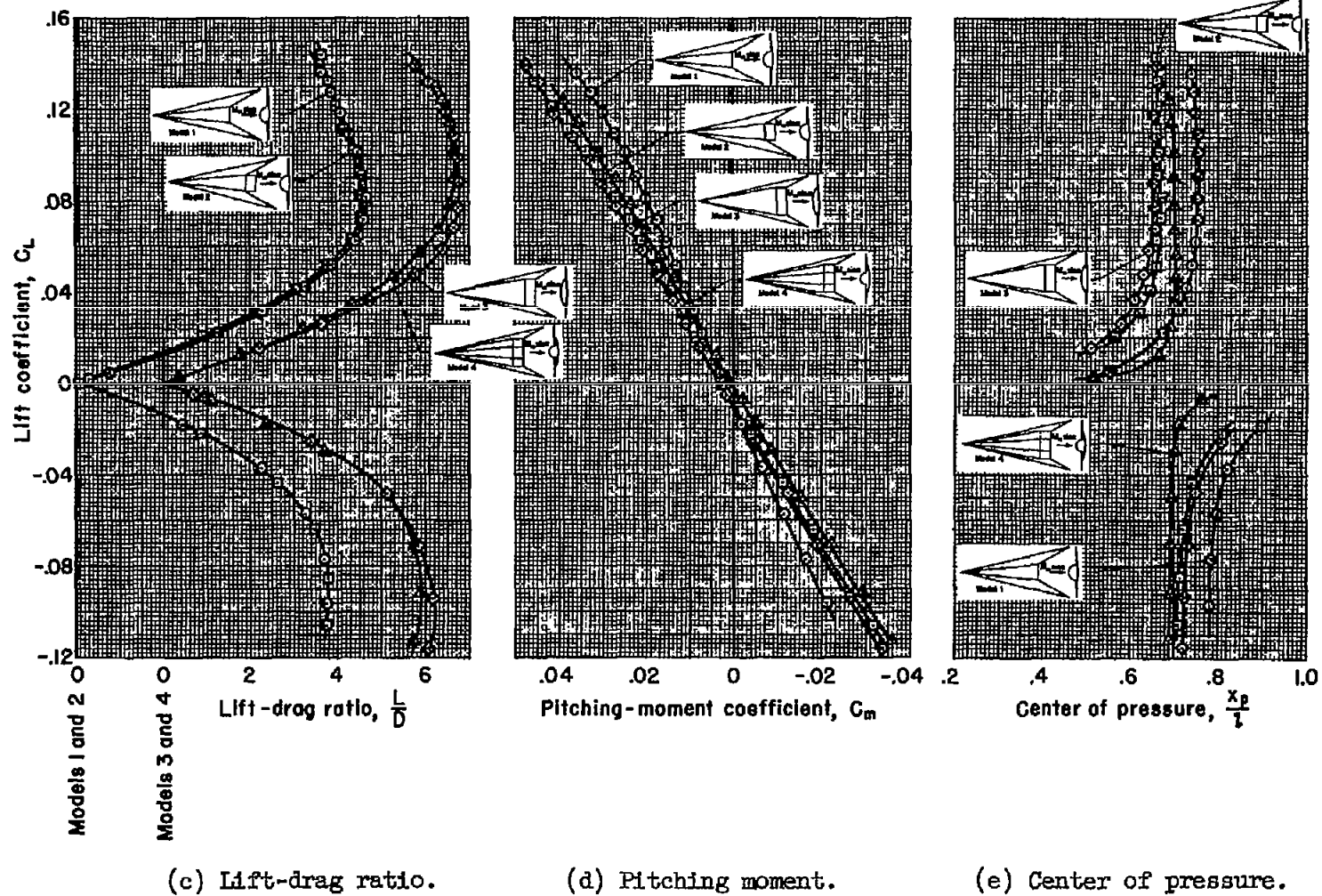


Figure 4.- Aerodynamic characteristics of arrow-winged configurations; $M_\infty = 3.88$, $R = 5.4 \times 10^6$.



(c) Lift-drag ratio.

(d) Pitching moment.

(e) Center of pressure.

Figure 4.- Concluded.

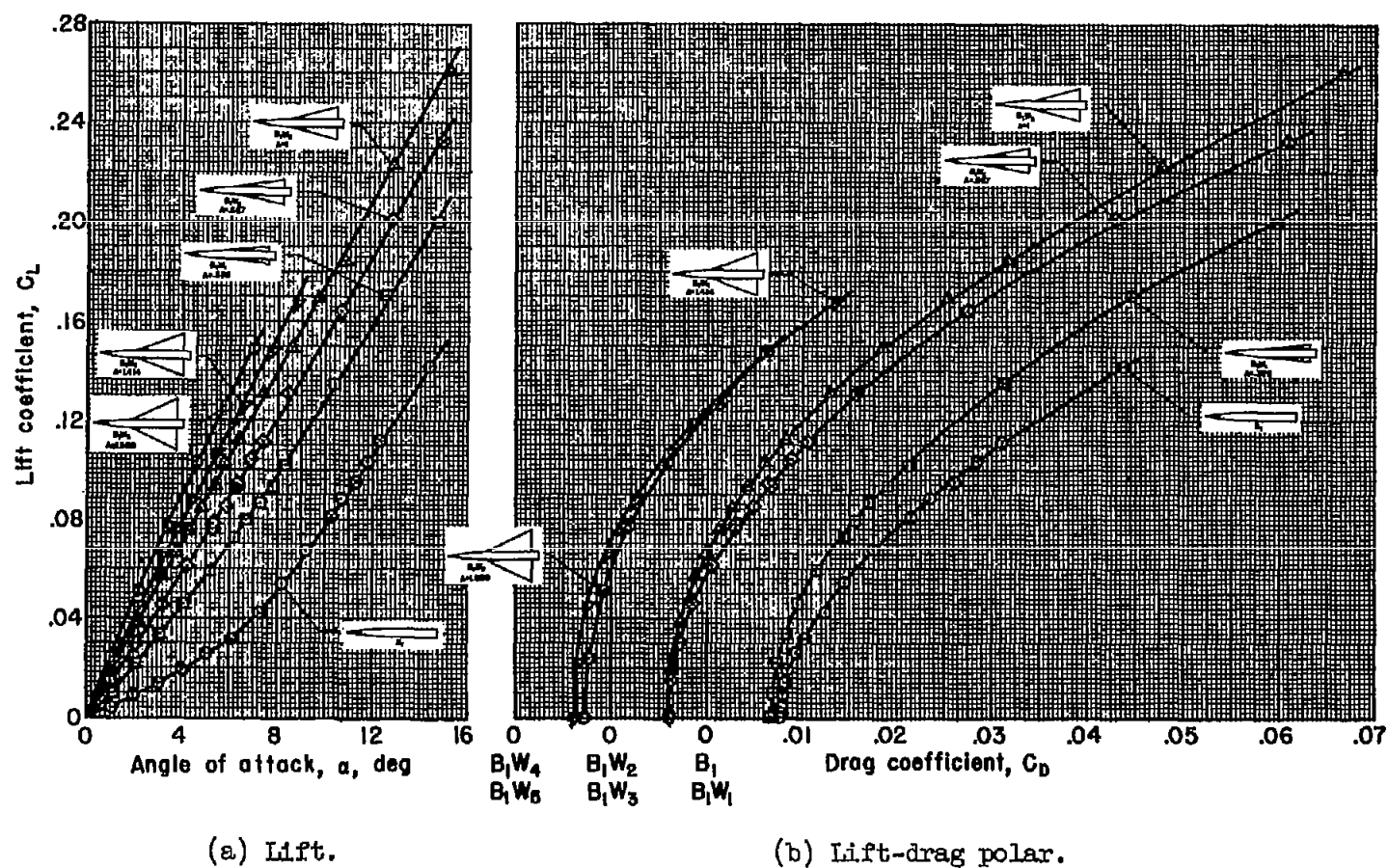


Figure 5.- Aerodynamic characteristics of triangular-winged configurations; $M_\infty = 2.94$, $R = 12.0 \times 10^6$.

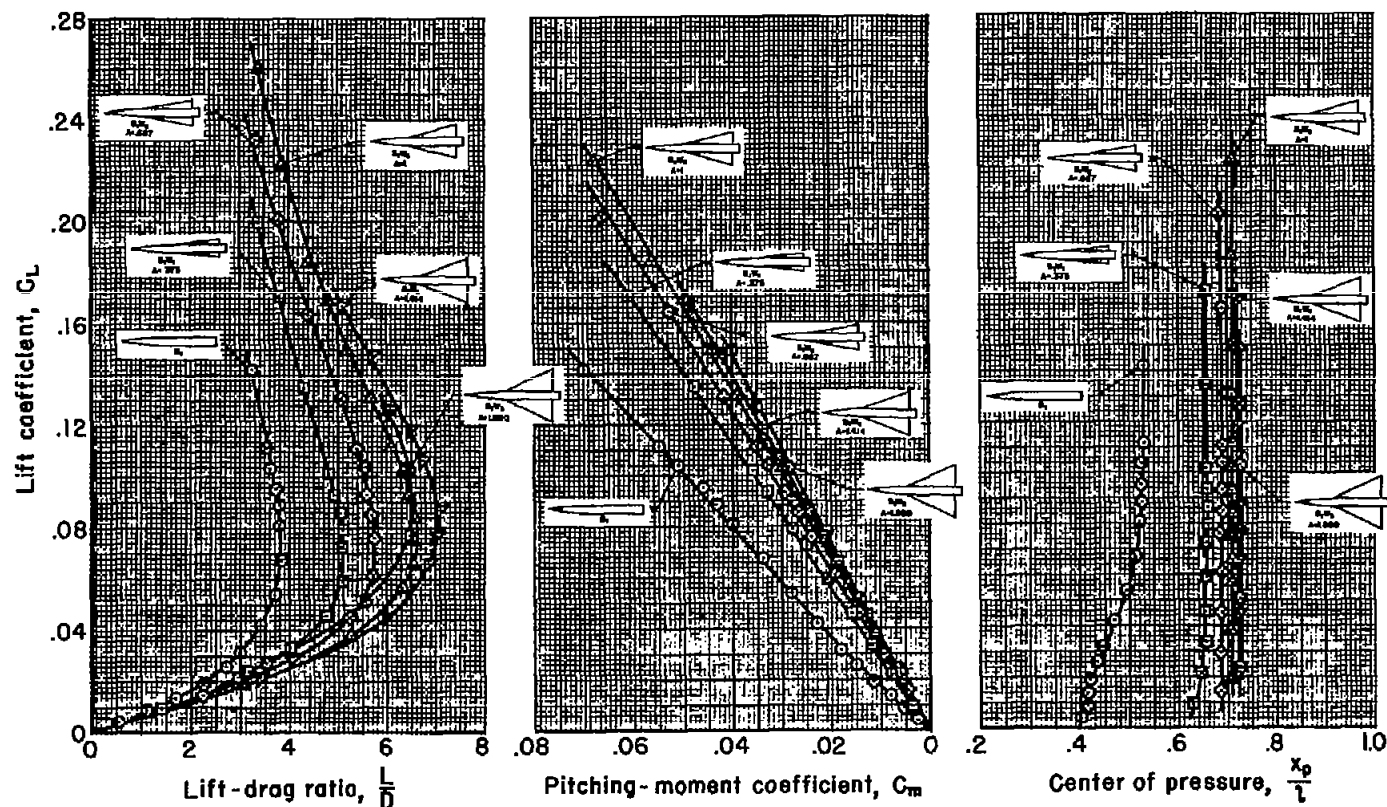


Figure 5.- Concluded.

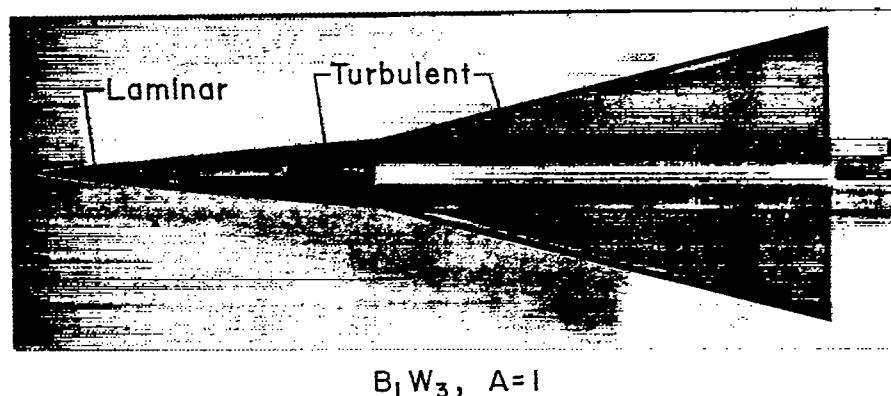
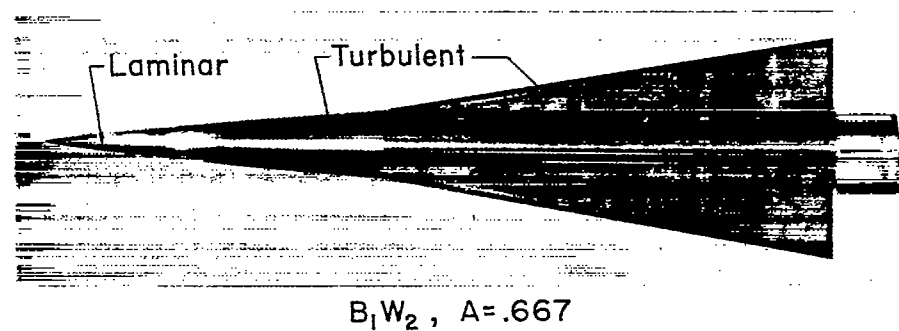
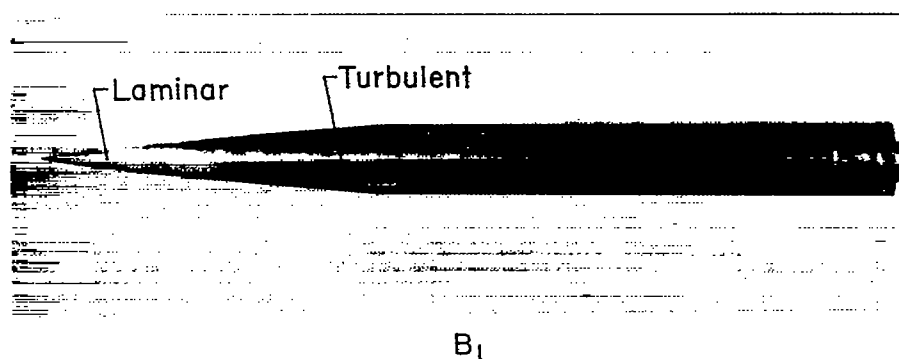


Figure 6.- Photographs of triangular-winged configurations taken following sublimation tests of models at $\alpha = 0^\circ$; $M_\infty = 2.94$, $R = 12.0 \times 10^6$.

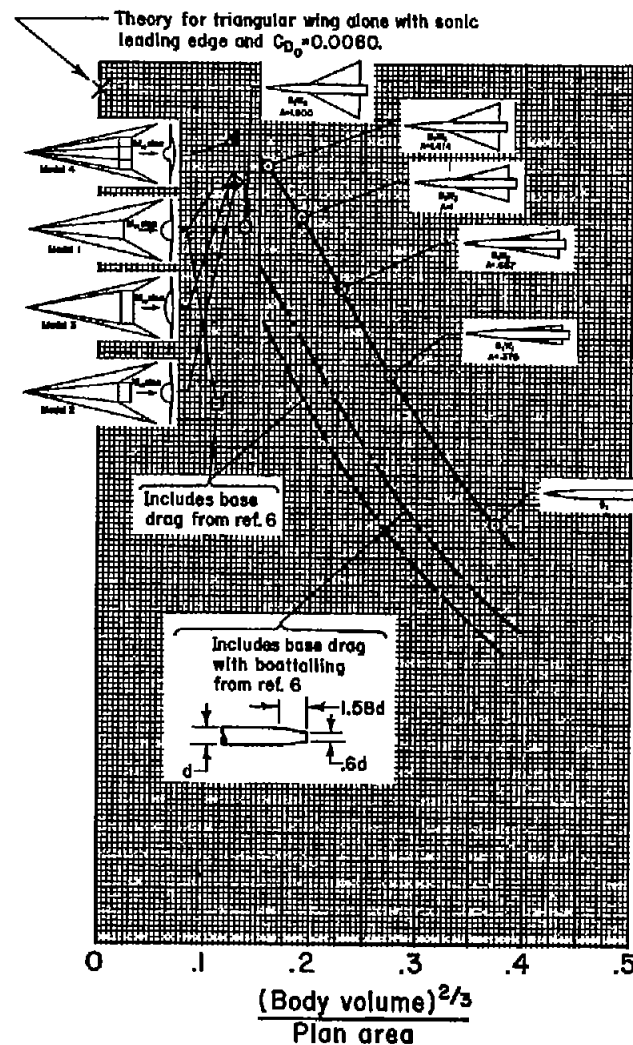
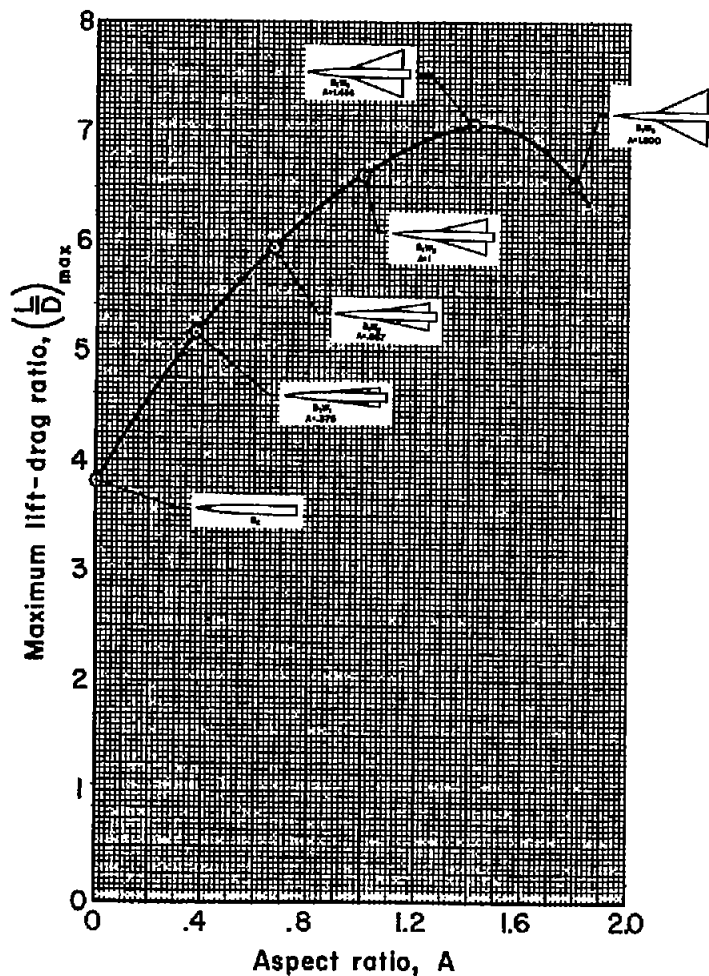


Figure 7.- Effect of aspect ratio and body volume on maximum lift-drag ratio; $M_{\infty} = 2.94$.